RSC Sustainability

ROYAL SOCIETY OF CHEMISTRY

PAPER

View Article Online
View Journal

Cite this: DOI: 10.1039/d6su00099a

Sustainable valorization of real polyurethane mattress waste *via* a novel multistage thermochemical approach

Mónica Calero, Adriana Parra-Marfil, Rafael R. Solís, Gabriel Blázquez* and Mario J. Muñoz-Batista *

This study explores pyrolysis as a sustainable route for the treatment and valorization of polyurethane-based mattress waste, a major contributor to urban landfill accumulation. It delivers a comprehensive assessment of the composition and properties of the products generated. The gaseous fraction, investigated through an *in situ* TGA/FTIR-MS scheme and GC, was found to be rich in methane, ammonia, hydrogen, and carbon dioxide, highlighting opportunities for both chemical synthesis and energy production, particularly *via* syngas generation. The liquid fraction, characterized by GC-MS and FTIR, contained a wide distribution of oxygenated compounds, aromatics, and hydrocarbons; simulated distillation further revealed its strong potential for applications in oil refining and chemical manufacturing. Detailed analysis of the solid fraction (XRD, XPS, N_2 physisorption, and elemental analysis) showed a carbon-rich material with promising applications as an adsorbent or solid fuel. Importantly, this fraction, together with the liquid product, was successfully employed as feedstock to prepare cobalt-based catalysts for a second step by a mechanochemical approach, which allows the production of a gas stream with competitive performance compared to reference catalysts prepared with commercial carbons.

Received 16th February 2026
Accepted 2nd June 2026

DOI: 10.1039/d6su00099a

rsc.li/rscsus

Sustainability spotlight

Polyurethane-based mattress waste, a major contributor to urban landfills, can be valorized *via* solvent-free pyrolysis, offering a fully integrated waste-to-resource strategy. The process converts all fractions into valuable products: the gas fraction, rich in H_2, CH_4, NH_3, and CO_2, is suitable for energy or chemical synthesis; the liquid fraction contains oxygenated compounds, aromatics, and hydrocarbons with potential in refining and chemical production. Less valorized fractions were transformed into cobalt-doped, N- and S-enriched carbon catalysts *via* a mechanochemical approach, enhancing syngas quality. This environmentally friendly route demonstrates a scalable alternative for sustainable treatment and comprehensive valorization of post-consumer polyurethane waste.

1. Introduction

The global consumption of plastics continues to increase due to their versatility, flexibility, durability, and low production cost, with annual production exceeding 359 million tons.[1] However, their extensive use has resulted in the massive accumulation of plastic waste, contributing significantly to environmental pollution due to their low biodegradability. Among the various types of plastic materials, polyurethanes (PUs) account for approximately 8% of total plastic production, making them the 6th most widely used polymer family. PUs are extensively applied in sectors such as construction, automotive, furniture and bedding, packaging, thermal insulation, and footwear.[2,3] PUs are generally categorized into two classes: foams (flexible or rigid) and CASE (Coatings, Adhesives, Sealants, Elastomers).[2] Flexible PU foams, which represent approximately 37% of global PU production, are mainly used in mattresses and automobile seats, whereas rigid foams, accounting for nearly 28% of global production, are primarily applied for thermal insulation purposes.[4,5] CASE PUs comprise around 35% of total PU production and are widely used in electronic products, ship structures, and shoes.[2,5]

PU-based materials are organic polymers with a wide variety of compositions, containing repeating urethane groups (–NH–(C=O)–O–) linking chemically distinct hard and soft segments.[6,7] These materials are synthesized through polycondensation reactions between polyisocyanates and polyols, which determine the final physicochemical and mechanical properties of the polymer.[8,9] The reaction between the isocyanate and hydroxyl groups results in the formation of the characteristic urethane linkage.[2,4,8] Furthermore, the incorporation

Department of Chemical Engineering, University of Granada, 18071 Granada, Spain. E-mail: gblazque@ugr.es; mariomunoz@ugr.es

of additives such as plasticizers, pigments, crosslinkers, and fillers, enables considerable modification of the structure and performance of PU-based products.[3] The widespread use of PU in products such as mattresses, insulation panels, furniture, automotive components, and packaging material, has inevitably led to the generation of substantial amounts of waste, most of which is currently landfilled. In this context, the European Association of Flexible Polyurethane Foam Blocks Manufacturers (EUROPUR) estimated 40 million of mattresses discarded in Europe in 2021,[10] corresponding to more than 300 kilotons of PU foam.[11,12] Nonetheless, the environmental and economic drawbacks linked to landfilling have raised interest in the development of sustainable recycling and recovery technologies for different waste streams, including PU waste.[13–15] There are four principal strategies for recycling PU foams: mechanical, chemical, thermochemical, and energy recovery processes through complete or partial oxidation.[16] Mechanical recycling is one of the most economical methods and involves grinding PU foams into particles suitable for secondary reprocessing in manufacturing applications.[4] In contrast, chemical recycling involves more complex and energy-intensive processes but allows the recovery of high-value products such as monomers and oligomers from the polymer.[17] Common chemical recycling techniques include glycolysis, hydrolysis, alcoholysis, aminolysis, ammonolysis, acidolysis, and phosphorolysis.[16] However, these methods often require relatively pure and homogeneous feedstocks, specific solvents or catalysts, and controlled operation conditions. By comparison, thermo-chemical processes such as pyrolysis, gasification, and hydrogenation have emerged as promising alternatives for converting waste into valuable chemicals and fuels, thereby supporting circular economy strategy.[16–20] Among these processes, pyrolysis has attracted considerable attention due to its versatility, operational simplicity, an ability to process heterogeneous and contaminated waste streams.[21] Pyrolysis is a thermochemical decomposition process conducted in the absence of oxygen, typically at temperature ranging 300–700 °C, depending on the feedstock nature and the target products.[22–26] During the thermal decomposition, three main fractions are generated: solid or char, liquid also named bio-oil or pyrolysis oil, and gaseous products composed mainly of light hydrocarbons and, in several cases, a syngas-like mixture.[27–29] The yield and composition of these fractions strongly depend on operational factors, such as heating rate, residence time, carrier gas composition, and reactor configuration.[26,30–33] Despite the relatively high energy demand, pyrolysis offers important advantages for PU waste management, including substantial volume reduction, recovery of energy and high-value products with limited pre-treatment requirements, and high versatility to process mixed or contaminated materials. Moreover, the gas released may partially feed the energy requirement, improving overall sustainability and industrial applicability. Although the literature reports several studies on PU recycling, many of these focus on transforming it into materials such as building or insulating materials.[34,35] Several studies focus on chemical recycling,[36–39] while thermochemical processes such as gasification or pyrolysis have received less attention.[40–42] Furthermore, there are very few analytical approaches involving waste mattresses.[40,43–46] A comprehensive analysis based on previous studies is presented in Table S1. In addition to identifying the main contributions reported in the literature on the use of waste mattresses as feedstock for pyrolysis processes, relevant information from mechanistic studies on PU structures is also included.[43,44,46–50] For instance, Garrido *et al.*[46] studied the pyrolysis behavior and degradation kinetics of PU mattress foam; however, their work mainly focused on gaseous emissions and did not include a detailed characterization of the liquid and solid products, as the analysis of the liquid (condensates) and solid fractions was not within the scope of their work. Serrano *et al.*[44] investigated the pressurized pyrolysis of mattress waste at temperatures up to 500 °C and pressures of 16.8 bar, primarily analyzing gaseous products such as CO, CO_2, CH_4, and H_2. Another relevant study investigated a two-stage scheme for the valorization of waste mattress foam, involving pyrolysis followed by thermal or catalytic cracking under an inert atmosphere.[43] In this work, pyrolysis was performed at 550 °C, followed by a secondary cracking stage at 300–800 °C using catalysts such as dolomite, olivine, and HiFUEL®.

This study provides a comprehensive evaluation of pyrolysis as a treatment and valorization of PU-based mattresses waste collected from the municipal solid waste landfill of Granada, Spain. Besides the detailed characterization of all pyrolysis products, *in situ* gas analysis (TGA–FTIR-MS) was performed to monitor the evolution of the pyrolysis process, providing valuable insights into the degradation behavior of real waste PU mattress materials. The study includes a detailed characterization of the original waste and the identification of key operating conditions for optimizing the pyrolysis process and the obtention of valuable product fractions. Within this framework, the gaseous fraction was identified as the most directly valuable stream. However, the liquid and solid fractions are not considered low-value residues; instead, they are redirected toward an alternative valorization pathway. To the best of our knowledge, this approach has not been previously reported. Specifically, both fractions are used as precursors for the preparation of a catalytic system *via* a mechanochemical approach, yielding a catalyst that enhances the properties of the gas fraction in a subsequent stage, leading to improved overall performance.

2. Experimental section

2.1. Materials

Real mattress waste, primarily composed of polyurethane, was supplied by the municipal solid waste treatment plant Ecocentral, located in Alhendín (Granada). A large volume of this bulky waste accumulates at the plant (Fig. 1A), where it is categorized based on the predominant component. A significant fraction (approximately 60%) consists of polyurethane (PU)-based structures, including mattresses designed with multiple layers (Fig. 1B) and those with a thick polyurethane layer (Fig. 1C), both featuring coatings, mainly polymers (PU, PE and PET) and textiles-based structures. For classification and processing, 20 polyurethane-based samples were collected,

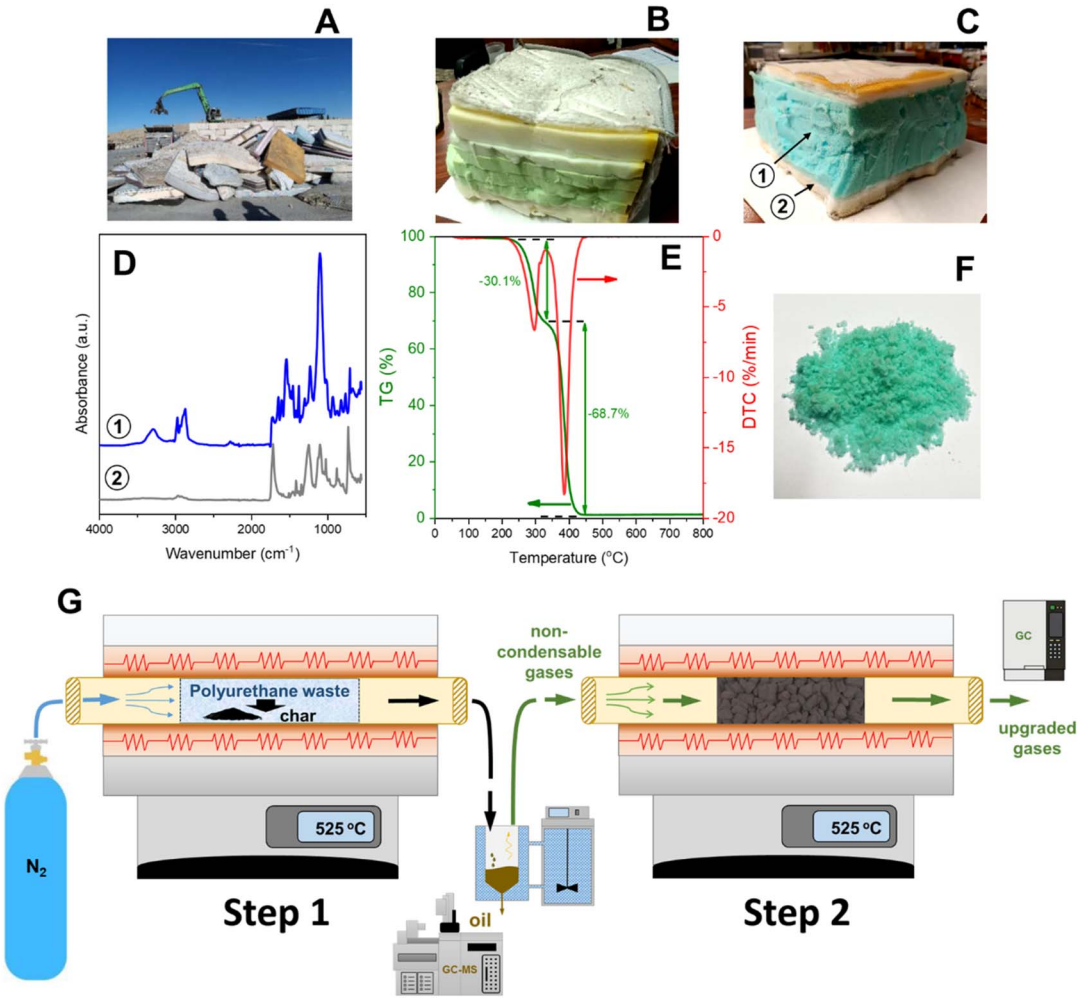

Fig. 1 (A) Representative image of the accumulation of end-of-life mattresses at the urban solid waste management company. (B, C and F) Images of polyurethane-based residual mattress samples. (D) FTIR spectra of representative sections of end-of-life mattress samples. (E) TGA results of the pyrolysis of polyurethane-based mattress samples. (G) Schematic representation of the reaction system. Step 1: pyrolysis. Step 2: catalytic transformation stage of non-condensable pyrolysis gases.

categorized, and labelled for study. The initial characterization and classification of the samples were performed through visual inspection, label analysis, and FTIR. The FTIR spectra were recorded between 550 cm^{-1} and 4000 cm^{-1} using a Spectrum 65 device from PerkinElmer. Fig. S1 of the SI shows details of this procedure. As a representative example, Fig. 1D shows the spectra corresponding to the expanded polyurethane and the coating of one of the discarded mattresses. Sample 1 corresponds to the polyurethane foam, while the coating (sample 2) allowed the identification of PU, PET, and PE, as previously discussed (Fig. 1C and D). The spectra obtained from other samples (PU and coatings) can be found in the SI (Fig. S2).

2.2. Pyrolysis assays

A preliminary analysis of thermal degradation under a controlled N_2 atmosphere was carried out by thermogravimetric analysis (TGA) (Fig. 1E), allowing the identification of a temperature range of interest between 400 °C and 600 °C. The TGA curves were obtained on a PerkinElmer STA 6000 thermobalance, setting around 10 mg of raw material per test. A parametric analysis was performed using a Box–Behnken experimental design, in which heating rate (5–15 °C min^{-1}), reactor residence time (30–90 min), and reaction temperature (400–600 °C) were selected as the independent variables. The design matrix consisted of 15 experimental runs, which enabled the evaluation of linear, quadratic, and interaction effects among the selected factors. To ensure statistical reliability and reproducibility, all experiments were conducted in triplicate, and the average values were considered for the subsequent response surface analysis. The design of experiments was further analyzed using a custom MATLAB script (MATLAB R2024b), allowing for efficient modelling and optimization of the process conditions. In addition, the pyrolysis process of the unprocessed structure and the samples processed to reduce their size (Fig. 1F) was evaluated, with no significant differences observed in the gas, solid, and liquid fractions yields. In addition, TGA/MS-FTIR analysis were conducted using a thermobalance of NETZSCH TGA/STA 449 F5 Jupiter, coupled with

a NETZSCH Aeolos QMS 403 Quadro quadrupole mass spectrometer and a BRUKER Invenio FTIR infrared spectrometer with a BRUKER TGA-IR gas cell. The signal intensity was normalized to the sample size and the carrier gas ion (m/z 40, Ar) to achieve a comparable ion current across different stages and between different samples, and to eliminate systematic instrumental errors.

As described in Fig. 1G, a horizontal fixed-bed tubular reactor from Nabertherm (model R 50/250/12) was used to carry out the pyrolysis experiments (step 1). The stainless steel 316 laboratory-scale reactor has an internal diameter of 4 cm and a length of 34.25 cm. A flowmeter was used for the controlled incorporation of inert N_2 flow. For each pyrolysis test, 20 g of sample was placed in a stainless-steel combustion boat (internal diameter of 2.73 cm and length of 30.6 cm). The temperature program consisted of increasing from room temperature to a final value at a heating rate of 10 °C min^{-1}. The final temperature was held for 1 hour under a constant N_2 flow rate of 0.8 L min^{-1}. The reactor was then allowed to cool down under a lower N_2 flow rate of 0.2 L min^{-1}. A condensation bath system with ethylene glycol at −7 °C was employed to condense and collect the liquid products in a glass bottle, defined in Fig. 1G as oil. Additionally, 2 L of gaseous product samples were collected in TEDLAR gas sampling bags every 15 minutes. The solid and liquid pyrolysis products were weighed as obtained, while the gas portion was determined by difference. The product fractions were calculated and expressed as weight percentages. The results were obtained in triplicate to determine the standard deviation of the measurements, accounting for error propagation.

The pyrolysis vapors obtained under the optimized conditions, corresponding to the maximum H_2 concentration, were subsequently submitted to a second catalytic stage (step 2), using a fixed-bed tubular reactor from Nabertherm (model R 50/250/12), as well (Fig. 1G), loading 5 g of catalyst under a packed-bed configuration.

2.3. Catalysts synthesis

The catalyst employed were synthesized by mechanochemistry using cobalt(II) nitrate hexahydrate ($Co(NO_3)_2 \cdot 6H_2O$, Sigma-Aldrich) together with the pyrolysis char and liquid fractions previously collected from the non-catalytic test. The amount of the Co precursor was fixed to obtain a material with 0.5 wt% relative to the carbonaceous support generated. The reaction mixture was inserted in a vibration ball-milling from Retsch MM400, equipped with a 50 mL stainless-steel jar and a 25 mm stainless-steel ball. The mixture was submitted to milling for 20 min under 30 Hz (ball-to-sample ratio of 10 : 1). After milling, the resulting material was calcined at 350 °C with a heating rate of 10 °C min^{-1}, followed by an isothermal treatment at the same temperature for 2 h, under a continuous N_2 flow.

A catalytic reference was prepared using the same mechanochemical protocol of synthesis but using as support a commercial carbon, with a surface area of 712.8 m^2 g^{-1} (PANREAC) named Co/C. Another reference was prepared using the commercial carbon and an impregnation and reduction protocol for the deposition of Pt nanoparticles (0.5 wt%). This last sample was prepared using an optimized laboratory procedure based on a chemical deposition process.[51,52] Briefly, a $NaBH_4$ solution (0.1 mol L^{-1}) was employed as the reducing agent for the metal precursor, with a fixed $Pt/NaBH_4$ molar ratio of 1 : 5. After the gradual dropwise addition of the $NaBH_4$ solution, the resulting material was separated by centrifugation, thoroughly washed with distilled water, and finally dried at 100 °C for 12 h. The resulting catalyst was named as Pt/C.

2.4. Characterization techniques

2.4.1. Solid samples: char and catalysts. The textural properties were evaluated by adsorption–desorption isotherms of nitrogen (N_2) at 77 K. The isotherms were registered using a Sync 200 apparatus from 3P Instruments. Before adsorption analysis, the samples were degassed at 110 °C under vacuum for 12 hours in a Prep J4 degasser unit from 3P Instruments. The specific surface area was calculated with the Brunauer–Emmett–Teller method (S_{BET}), and the total pore volume (V_T) was estimated from the nitrogen uptake at a relative pressure of $P/P_0 \approx 0.99$.

The crystalline properties were analyzed by X-ray Diffraction (XRD) in a Bruker D8 Discover diffractometer equipped with a Pilatus3 R 100K-A detector. The diffraction patterns were measured at 25 °C with Cu Kα radiation ($\lambda = 1.5406$ Å) and the spectra were processes with QualX software to identify the crystalline phases.

The chemical composition of the bulk was analyzed by elemental analysis and while at surface level was conducted by X-ray photoelectron spectroscopy. CHNS elemental analysis was conducted in a TruSpec device, micro model from LECO. X-ray Photoelectron Spectroscopy (XPS) were registered in a Kratos Axis Ultra-DLD (Delay Line Detector) with an X-ray source emitting Al Kα radiation. High-resolution spectra were obtained for C 1s, N 1s, and O 1s XPS regions. The C 1s peak at 284.6 eV was used as a reference to correct the positions of the other measured regions. Data processing was performed with XPSpeak 4.1® software, applying a Shirley-type baseline correction.

The morphology was assessed by Scanning Transmission Electron Microscopy (STEM) using a Thermo Fisher Scientific Talos F200X G2 microscope (operating at 20–200 kV), equipped with a High-Angle Annular Dark Field (HAADF) detector and an Energy-Dispersive X-ray (EDX) analysis system (Bruker X-Flash 6T-30).

2.4.2. Liquid samples: oils from pyrolysis. Simulated distillation was performed to determine the boiling point distribution of oil fractions. The analysis was performed in a PerkinElmer Clarus 590 chromatograph equipped with an Elite 2887 capillary column, following the principles of ASTM D2887. The samples were directly injected into an ELITE 2887 capillary column measuring 10 m in length, with an inner diameter of 0.53 mm, and a film thickness of 2.65 μm. Detection was carried out using a flame ionization detector (FID). Calibration was performed with a certified standard of n-paraffin mixture (ASTM D2887-12 from ResteK) covering from C_5 to C_{44}.

Data acquisition and boiling point distribution calculations were processed using instrument software, and results were reported as cumulative weight percent recovered *versus* equivalent atmospheric boiling temperature.

FTIR technique was also applied to tentatively identify the main functional groups present in the pyrolysis oils. FTIR spectra were recorded in a PerkinElmer Spectrum 65 device in the range of 550–4000 cm^{-1}.

Additionally, Gas Chromatography-Mass Spectrometry (GC-MS) was employed to identify compounds of the liquid fraction. For the analysis, a ZB-5MS Phenomenex capillary column (30 m × 0.25 mm ID, 0.25 μm film thickness) was used within an Agilent 7890A high-resolution GC paired with a Waters triple quadrupole mass spectrometer. The injector and transfer line temperature were set at 250 °C, with the injector in split mode. Helium was used as a carrier gas with a flow rate of 1 mL min^{-1}. The mass spectrometer settings included an interface temperature of 250 °C, full scan mode from 30 to 650 Da, and electron ionization energy of 70 eV. Compound identification was achieved using the National Institute of Standards and Technology (NIST) mass spectrum library, with NIST MS Search 2.0 software integrated with MassLynx V4.1 software and the NIST 08 mass spectrum library.

2.4.3. Gas samples: pyrolytic gas. The gas phase was examined using an Agilent gas chromatograph model 990 Micro GC, which features two channels and a thermal conductivity detector. The first channel was linked to a Molsieve 5 Å column (20 m × 0.25 mm, ID 30 μm) coated with a molecular sieve, while the second channel was coupled to a PoraPLOT column (10 m × 0.25 mm, ID 8 μm). This system facilitates the analysis and tracking of the reaction by measuring non-condensable products, such as hydrogen, carbon dioxide, carbon monoxide, ammonia, methane, and C_2–C_3 hydrocarbons, as the pyrolysis progresses.

3. Results and discussion

3.1. Pyrolysis experiments

As aforementioned, the pyrolysis experimental study was carried out of several mattress samples whose main component was polyurethane. With the aim of identifying the contribution of the major component to the products, the mattresses were separated into their fractions, and representative samples were subjected to thermal treatment. The importance of studying pure polyurethane structures is also supported by the existence of a large number of uncovered mattresses or large pieces of polyurethane foam accumulated in landfills. The evaluation of produced product fractions utilized four polyurethane samples (PU_A, PU_{B1}, PU_{B2}, and PU_{B3}), as well as two coating samples (C_A and C_B) derived from discarded mattresses (Fig. S1). The sample PU_A corresponds to a monolayer polyurethane form (Fig. 1C and S1), while the PU_{B1}, PU_{B2}, and PU_{B3} samples are derived from multilayer mattresses (Fig. 1B and S1). The pyrolysis results in terms of weight% fraction for gas, char, and liquid are shown in Fig. 2A. The polyurethane samples (PU_A, PU_{B1}, PU_{B2}, and PU_{B3}) exhibited average wt% of 12.6% (SD = 2.2), 55.6% (SD = 4.1), and 31.8% (SD = 3.1) for char, liquid, and gas, respectively. These results indicate a predominance of liquid products, with a relatively lower production of char and non-condensable gases. The pyrolysis of the mattress coatings, composed of a polymer blend that is also suitable for pyrolysis, was studied under the same conditions. The coating samples (C_A and C_B), which are based on a mixture of polyurethane, polyethylene terephthalate (PET), and polypropylene (PP), displayed average yields of 23.5% (SD = 0.2) for char, 39.1% (SD = 1.2) for liquid, and 37.4% (SD = 1.4) for gas. The differences in the pyrolysis products between the polyurethane foam samples and the mattress coatings can be attributed to the distinct compositions of the materials. The polyurethane foam samples (PU_A, PU_{B1}, PU_{B2}, and PU_{B3}) are composed of polyurethane, a polymer known for its relatively low molecular weight and higher volatility when subjected to pyrolysis. On the other hand, the mattress coatings (C_A and C_B), which are composed of a mixture of polyurethane, PET, and PP, produce more char and gas. PET and PP have higher molecular weights and more stable structures compared to polyurethane, which leads to the formation of more char. In the following sections, a comprehensive analysis of each fraction is provided. Fig. 2B shows the influence of temperature (400, 500, and 600 °C) on the products obtained (liquid, solid, and gas fractions) for the PU_A sample. With increasing temperature, the most significant changes correspond to a reduction in the amount of solid obtained above 500 °C. This trend is consistent with the results obtained from TGA (Fig. 1E). The results shown in Fig. 2A were obtained under the operating conditions that maximize the H_2 content in the gas fraction (temperature: 525 °C, heating rate: 13.1 °C min^{-1} and time: 60 min). This outcome is particularly desirable since, as discussed throughout the manuscript, the gas fraction represents the most attractive stream for the valorization of these residues, especially when considering the impurities identified in the solid and liquid fractions. As described in the Materials and methods section, this optimization was carried out through a Design of Experiments (DOE) considering the main variables influencing the pyrolysis process. The response surfaces obtained are presented in Fig. 2C–E. Each plot depicts the hydrogen percentage profiles as a function of two varying factors, while the third was held constant at its central value.

3.2. Gas fraction

To analyze the thermal decomposition steps of polyurethane residues from mattresses and to determine the temporal progress of gas compounds formed, Fig. 3A presents the molar concentration of gases compared to their initial molar concentrations. The black line represents the ratio of the number of gases produced at a given time to the initial number of gases. It demonstrates the rapid degradation of the polyurethane waste sample at the working temperature. The maximum gas production occurred within the first 5 minutes of the reaction, indicating the highest rate of degradation. By 60 minutes, the degradation was almost complete, with the production of non-condensable gases constituting less than 5%. Additionally, Fig. 3A shows the highest production rates of CH_4 and CO_2. Conversely, H_2 exhibits a slower rate of

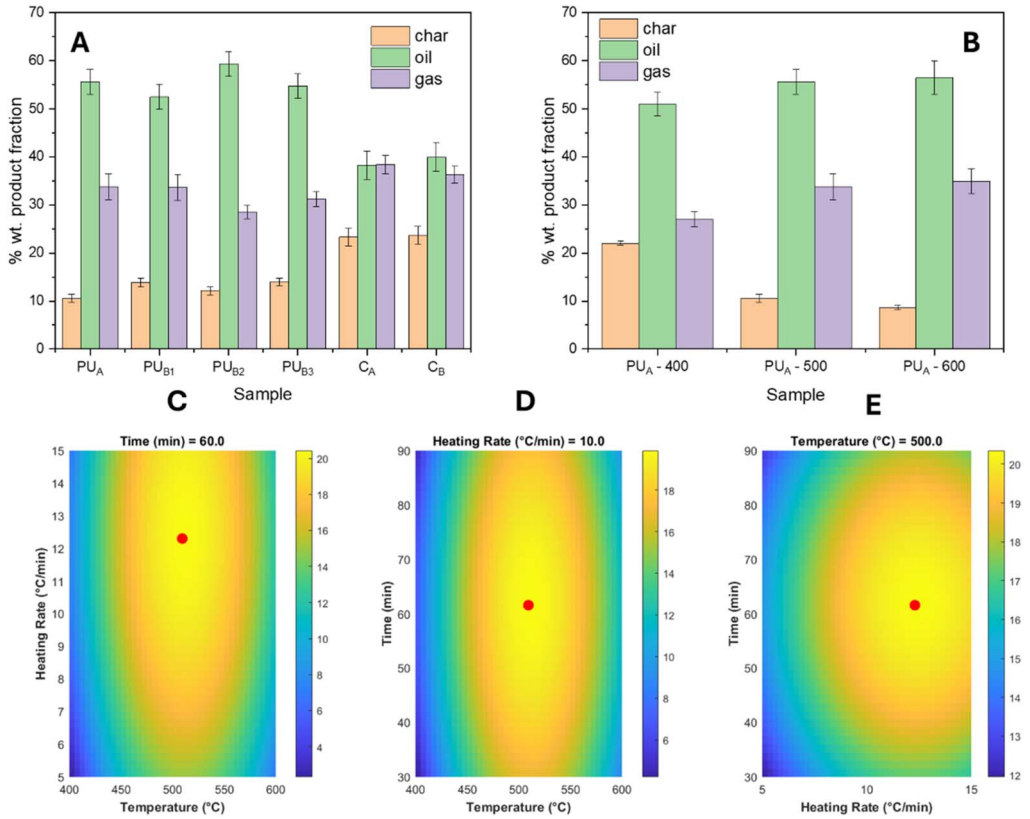

Fig. 2 (A) Weight percentage distribution after pyrolysis of the studied residual polyurethane mattress (PU$_A$, PU$_{B1}$, PU$_{B2}$ and PU$_{B3}$) samples and the coatings (C$_A$ and C$_B$). (B) Influence of the temperature on the distribution of fractions (char, liquid and gases) obtained during the pyrolysis, (C–E) response surfaces used to identify the maximum H_2 concentration in the gas fraction.

production, which can be attributed to the complexity of decomposition reactions. Fig. 3B presents the amounts (expressed in molar percentages of produced gas) of each detected compound (CH_4, NH_3, CO_2, H_2, CO, and grouped C_2- and C_3-compounds). The data revealed that the major compounds produced were (molar%) CH_4 (38.7%), CO_2 (22.8%), and H_2 (18.2%). Methane and hydrogen are typical products of the thermal decomposition of polyurethane-related materials, as well as carbon dioxide, related to the oxidation of carbon-containing compounds.[42,53] A relevant amount of C_2-components were detected, associated with the generation of C_2H_2 (0.7%), C_2H_4 (1.7%), and C_2H_6 (4.1%). The contribution of C_3-compounds is exclusively associated with C_3H_4. As described in Fig. 3A and B, the main nitrogenous compound detected was ammonia, which is the primary product generated by the decomposition of amines and urethane groups formed from the degradation of the isocyanate component.[53–55] Hydrogen cyanide was detected at very low concentration (non-quantifiable traces), which is commonly associated with degradation from the fragmentation of isocyanate groups (–N=C=O) and other nitrogenous structures such as urea and urethane derivatives.[56,57]

The pyrolysis of the sample was studied using thermogravimetric analysis (TGA) coupled with mass spectrometry (MS) and Fourier-transform infrared spectroscopy (FTIR). The data obtained provides a comprehensive understanding of the thermal decomposition process and the evolution of gaseous products. Fig. 3C presents the ion current (IC) as a function of mass-to-charge ratio (m/z) and temperature. It is observed that gases are generated primarily between 350 °C and 450 °C, which aligns with the description of the TG profile.[53,54] To facilitate the analysis, specific mass-to-charge ratios (m/z) were identified to track the evolution of gases such as H_2, CH_4, CO, CO_2, C_xH_y, and NH_3. This selection, illustrated in Fig. 3D, is based on literature data,[14,42,45,58] and corroborated by the identification by GC of the main products discussed in Fig. 3A and B. The identification facilitates a detailed analysis of the gaseous products formed during pyrolysis. From the MS data, it is evident that CO_2 is the first compound to be produced. This early production of CO_2 is consistent with the first significant mass loss of 30.1% in the TG analysis (Fig. 3C). The initial decomposition around 250 °C involves the breakdown of weak chemical bonds, leading to the release of small volatile compounds, primarily CO_2 (m/z 44). The gas profile exhibits a maximum, a common behavior in pyrolysis analyses where the sample undergoes thermal decomposition. This maximum indicates the peak rate of gas evolution during the pyrolysis process and is observed as a negative peak in the DTG curve (Fig. 1E), indicating a rapid decomposition phase that leads to the release of CO_2. This temperature marks the onset of significant thermal degradation, which continues with a slower degradation process between 300 °C and 400 °C associated with a maximum in the DTG curve (% min^{-1}) shown

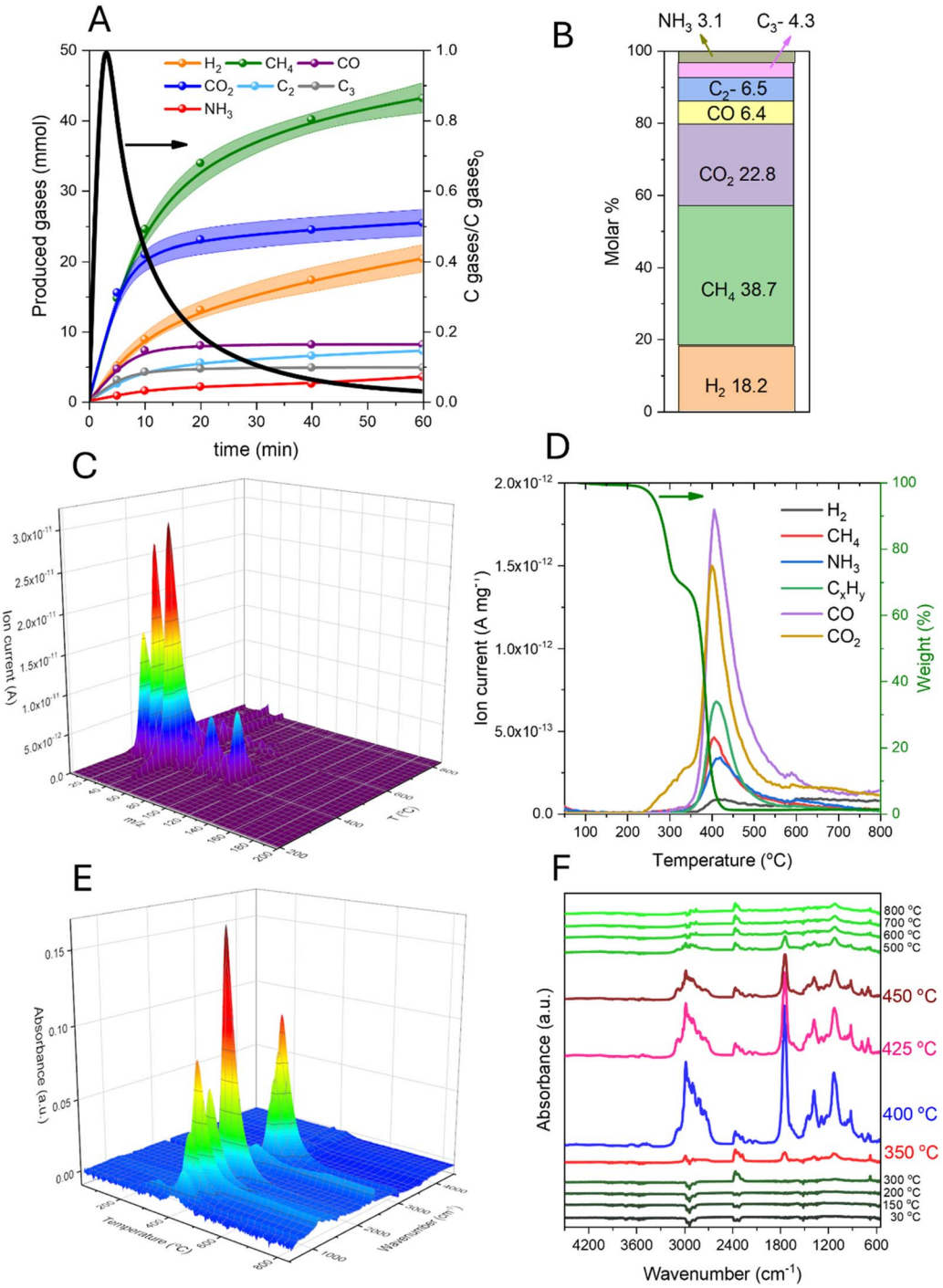

Fig. 3 (A) Temporal production of non-condensable gases obtained from the pyrolysis of polyurethane-based mattress waste. Non-condensable produced gases and initial gases concentration ratio obtained during the pyrolysis. (B) Concentration of non-condensable gases expressed in molar% obtained at the end of the reaction (1 hour). The experimental error for all data was <6%. As an example, the error (shaded area) for the compounds CH_4, H_2, and CO_2 is included in (A). (C) 3D MS spectra measured for each m/z and temperature value during the pyrolytic degradation of a polyurethane-based mattress waste sample. (D) Generation of the most representative species (identified by specific m/z value) produced during the reaction. (E) 3D FTIR spectra as a function of temperature. (F) Selected FTIR spectra at different temperatures.

in Fig. 1E. During this phase, urethane linkages cleave into isocyanates and alcohols.[54] This phase is followed by a pronounced weight degradation of 68.7% which concludes at 450 °C, indicating the complete breakdown of the material, which is also shown as a negative peak in the DTG curve (Fig. 1E). This degradation process results in the formation of CH_4 (m/z 16) and other light hydrocarbons (C_2–C_3) (m/z 26), CO (m/z 28), and amines (m/z 30).[42,53,54] The amines further

decompose into ammonia (m/z 17). This contribution may overlap with the signal from water (H_2O), which appears at m/z 18 and may be released along with volatile compounds in the initial phase, as highlighted by other authors.[57,59]

Fig. 3E presents the FTIR spectra obtained as a function of temperature, providing valuable information on the functional groups present in the evolved gases. Fig. 3F includes representative spectra at various temperatures, highlighting the key absorption bands, which support the identification of various compounds generated with the rise in temperature. Negative bands in the FTIR spectrum, observed principally up to 200 °C, indicate a decrease in the absorption of certain molecular vibrations, which is attributed to the loss of functional groups such as methyl and methylene (C–H stretching vibration bands at 2870–2972 cm^{-1}),[54,60] hydroxyls (O–H stretching vibration bands at 3500–3700 cm^{-1}, and O–H bending vibration at 1336–1555 cm^{-1}),[60,61] carbonyls (C=O stretching vibration bands at 2290–2400 cm^{-1}, and bending vibration at 700 cm^{-1}),[60,62] and other volatile organic groups that decompose and release gases such as CO_2 and H_2O. Conversely, with the increase in temperature above 300 °C, carbonyl bands (2290–2400 cm^{-1} asymmetric stretching and 700 cm^{-1} bending vibrations) emerge, confirming the early identification of CO_2 by MS.[48,54,60,62]

When the temperature reaches about 350 °C, the soft segment of polyurethane undergoes thermal breakdown, forming esters or anhydrides through the degradation or oxidation of the polyol components. The presence of esters and anhydrides is supported by the surge of the band around 1750 cm^{-1},[4,63,64] attributed to their C=O stretching vibration, and the coexisting appearance of C–H stretching vibration bands in the 2890–2980 cm^{-1} region, which are characteristic of aliphatic CH_2 and CH_3 groups generally found in the polyol backbone or in esterified degradation products.[8,65] Furthermore, the growing absorbance in the C–O stretching region (1110–1380 cm^{-1}) offers complementary evidence for the existence of ester functionalities.[8,46,65]

In concordance with the results of MS–TGA, FTIR spectra notably exhibit the following phase of isocyanates and alcohols formation from the thermal cracking of urethane linkages. The occurrence of isocyanates is typically detected at higher temperatures (above 350 °C) *via* their characteristic –N=C=O stretch vibration around 2270 cm^{-1}.[4,46,66] The increase in absorbance at 1500 cm^{-1} due to N–H bending vibration,[4] and the intensity increase of the 1750 cm^{-1} band (C=O stretching vibration) are associated with the presence of urethane groups.[65] The presence of C–O bands at 1009 and 1227 cm^{-1} due to stretching vibration,[54,64] the C–H bending vibration band at 1460 cm^{-1},[64] and stretching vibration bands at 2700–2800 cm^{-1},[54] along with a broad O–H stretching band in the 3600–3700 cm^{-1} region,[48,54] suggest the generation of alcohols from polyol fragmentation. Further decomposition of polyols and urethanes and their fragments may lead to the release of CO, as previously observed in MS–TGA analyses. The occurrence of CO is confirmed by the rotational–vibrational bands around 2100–2200 cm^{-1}.[48,67] The broad band at 3490 cm^{-1} is associated with N–H stretching,[4,46] suggesting the presence of ammonia (NH_3) primarily produced from urea and amines. The shoulder at 3086 cm^{-1} and the intense peak at 2981 cm^{-1} are indicative of aromatic and aliphatic hydrocarbons, respectively.[54] The reduction in the peak intensities of FTIR spectra with pyrolysis progression, similar to the MS data, indicates the progressive consumption and decomposition of the compounds as the temperature increases. This trend is typical in pyrolysis studies, where the initial sharp peaks gradually diminish as the volatile components are released and decomposed.[14]

3.3. Liquid fraction and solid fraction

Based on the results obtained by GC-MS in combination with the FTIR analysis of the liquid phase (Fig. 4A) it is possible to provide a description of the structure. As can be seen in Fig. S3, the GC analysis (GC-MS) of the liquid phase revealed a complex mixture, with a wide range of peak contributions of oxygenated compounds, aromatics, and hydrocarbons, indicating the formation of structurally diverse products. In addition, the FTIR analysis further supports this structural assessment, offering complementary insights into functional group composition. Based on the results obtained by GC-MS in combination with the FTIR analysis of the liquid produced, the broad absorption band between 3735 cm^{-1} and 3072 cm^{-1} indicates the presence of hydroxyl (–OH) and amine (–NH) functional groups, suggesting the presence of residual polyols or degradation products from the urethane linkages.[46,60,61] Peaks at 2971, 2933, and 2871 cm^{-1} correspond to C–H stretching vibrations from aliphatic hydrocarbons, supporting the presence of alkyl chains, as observed in compounds like polyethylene glycol oligomers or polyethylene oxide chains. The strong absorption at 1712 cm^{-1} is characteristic of carbonyl (C=O) stretching, indicating the presence of ketones, esters, or carboxylic acids, aligning with the detection and identification by GC-MS of phenylacetic acid and 2-propanone, 1-(1-methylethoxy) ($C_6H_{12}O_2$). The band at 1623 cm^{-1} suggests C=C stretching, confirming the presence of aromatic or conjugated systems,[68] in line with the identification of cyclooctatetraene-like structures (C_8H_8). The peak at 1511 cm^{-1}, typically associated with aromatic ring vibrations, supports the presence of benzene derivatives such as 4-phenylbutanenitrile and 2-phenylethanamine, *N*-methyl-α-phenylethylamine, all of which were unequivocally identified by mass spectrometry. Peaks at 1449, 1371, and 1332 cm^{-1} can be associated with C–H bending vibrations, indicating alkyl substituents.[64] The absorption at 1254 cm^{-1} suggests C–O stretching from ether or ester groups, in agreement with the detection of 2-ethoxy-1-methoxyethoxy and 2,2-dimethoxybutane. The peaks at 1082 and 1004 cm^{-1} indicate the presence of C–O–C ether linkages, supporting the decomposition of polyether polyols.[69] The absorptions at 915, 781, and 697 cm^{-1} correspond to out-of-plane bending vibrations of aromatic rings and alkene groups,[68,70] reinforcing the presence of aromatic compounds and unsaturated hydrocarbons. Elemental analysis (CHNS) confirmed the presence of these elements in the liquid fraction. The obtained oil contains 56.1%, 7.91%, 4.67%, and 0.01% of C, H, N, and S,

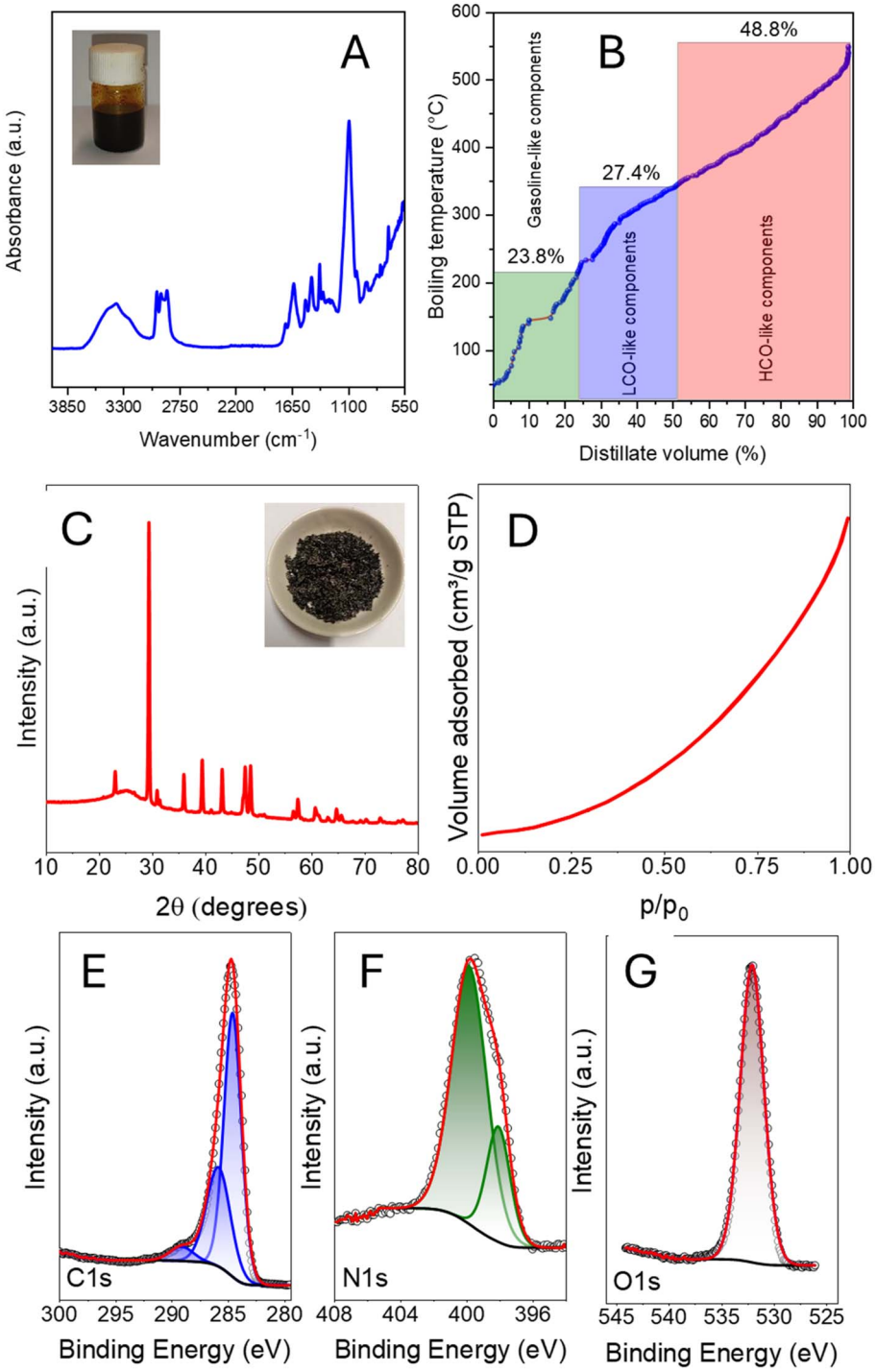

Fig. 4 Characterization of the liquid and solid fractions obtained from pyrolysis. (A) FTIR spectra of the liquid fraction obtained during the pyrolysis of the residual mattress sample. (B) Simulated distillation data and grouped components. Distribution of the products analogous to the common cuts used in petroleum refining processes. (C) XRD diffraction pattern, (D) N_2 physisorption isotherms and XPS high-resolution spectra of C 1s (E), N 1s (F), and O 1s (G).

respectively. The diversity of functional groups and molecular structures suggests multiple potential valorization routes, emphasizing the need for further analytical characterization and refinement strategies to optimize the pyrolysis process and identify feasible applications such as chemical feedstocks, fuel precursors, or chemical production.

While identifying the structural composition of the liquid phase is crucial, its comparison with conventional fuel fractions from petroleum refining provides insight into its potential applications.[14,71] As can be seen in Fig. 4B, simulated distillation data (expressed in volume%) indicates that 23.8% of the pyrolyzed liquid consists of compounds with boiling points comparable to gasoline, 27.4% aligns with light cycle oil (LCO), and 48.8% corresponds to heavy cycle oil (HCO). A more detailed breakdown of boiling point ranges indicates that the liquid contains fractions like light naphtha (5.2%), medium naphtha (2.6%), heavy naphtha (13.8%), kerosene (11.2%), distillate fuel oil (18.8%), light vacuum gas oil (33.5%), and heavy vacuum gas oil (14.9%). Despite these similarities in boiling ranges, significant structural differences exist between the pyrolyzed liquid and petroleum-derived fractions. Petroleum-based fuels predominantly consist of saturated and unsaturated hydrocarbons,[71] whereas the pyrolyzed liquid contains a substantial fraction of oxygenated and nitrogen-containing compounds due to the degradation of polyurethanes. The presence of polyols, esters, and amines in the pyrolysis oil influences its chemical stability, combustion properties, and suitability for further upgrading processes. These differences suggest that while direct application as a fuel may be challenging, refining or catalytic upgrading could enhance its compatibility with existing fuel streams.

The char obtained from the polyurethane foam mattress submitted to pyrolysis was characterized by its structural, chemical composition, and textural properties. The elemental analysis of the char indicated the following composition (molar%): 73.0% of C, 3.3% of H, 13.0% of N, and 0.02% of S. The XRD diffraction pattern, see Fig. 4C, revealed the presence of calcium carbonate, concretely, calcite. Usually, the mechanical properties of foam mattresses are enhanced with several additive fillers. The most common are inorganic chemicals such as calcium carbonate, aluminum silica, titanium dioxide, and talc.[72–74] During the pyrolysis, the $CaCO_3$ was concentrated in the solid, and due to the temperature of the thermal process, *e.g.* 525 °C, the thermal decomposition was not triggered.

The textural properties of the solid were explored by N_2 adsorption at 77 K. Fig. 4D depicts the isotherm, which describes a type III, where no identifiable monolayer is reached, and the weak interactions on the surface, characteristic of a material with a poor surface area 2.2 $m^2\ g^{-1}$ and low mesoporous volume 0.011 $cm^3\ g^{-1}$.

Further analysis was conducted on the chemical composition at the surface by XPS, focused on C, N, and O, as illustrated in Fig. 4E–G. The spectrum of C 1s was interpreted by deconvolution in three contributions, the most prominent at 284.6 eV attributable to sp^3 C–C; the second one placed at 286.0 eV, which could explain the presence of C–O responsible of carbon in ether, hydroxyl bonded C, or C associated with ether bond in lactone/esters; and finally a third much less intense located at 289.1 eV, characteristic of carboxyl, lactone or ester groups.[75] The analysis of N 1s spectrum was explained with two contributions located at 399.5 eV and another secondary, less intense, placed at 398.0 eV. The first one could explain the presence of amide and nitrile groups,[76] while the second one could be attributed to the presence of pyridine groups.[76,77] The analysis of O 1s led to a highly symmetric peak centered at around 532.5 eV, the typical value either and hydroxyl groups bonded to aliphatic and carbonyl.[75]

3.4. Valorization of fractions and enhancement of the properties of the gas stream

As discussed previously, the presence of nitrogen and sulfur species in both the liquid and solid fractions severely limits their direct application potential. For instance, pyrolysis oils containing significant amounts of heteroatoms (N, S, O) are incompatible with conventional petroleum refinery lines, as their high reactivity, corrosivity, and tendency to produce undesired emissions hinder direct integration into established refining infrastructures. A similar limitation is encountered for the solid char. Moreover, its intrinsically low surface area further limits its potential use as an adsorbent unless subjected to additional activation treatments. In contrast, the gaseous fraction shows higher immediate value for energy applications, but its composition often requires improvement. One of the main upgrading strategies focuses on increasing the hydrogen content.[24,78–82] Upgrading of gaseous streams is commonly carried out through catalytic processes, highlighting the relevance of developing efficient catalytic systems capable of integrating within a closed valorization scheme. In this context, the solid and liquid fractions can be employed not as direct fuels but as precursors and reactive agents in the synthesis of novel catalytic materials, closing the loop of waste valorization. Following this rationale, the contribution proposes an innovative strategy in which the pyrolysis char and oils are used as sources of C, N, S, and O during the preparation of a Co-based catalyst. Through a mechanochemical route, a carbonaceous catalytic material is produced, doped with O and N, and decorated with surface Co_3O_4 nanoparticles. Materials based on Co_3O_4 have been widely reported as active catalysts in several relevant catalytic processes, including oxidation reactions (*e.g.*, CO oxidation and volatile organic compound abatement), reforming and hydrogen production reactions.[83–85] Additionally, sulfur species initially present in the char and oils are retained within the structure and have been reported to positively contribute to catalytic activity in certain reactions.[86–88] The resulting material thus represents a multifunctional catalyst derived from waste fractions, avoiding the use of solvents or additional reagents.

Fig. 5 shows the structural and compositional features of the synthesized catalyst. STEM and EDX mapping reveal a relatively homogeneous distribution of C, N, and O throughout the material, while cobalt oxide phases are preferentially deposited at the surface and edges, coinciding with areas of higher sulfur concentration. Importantly, this catalyst was obtained *via* a mechanochemical route without the addition of solvents, underscoring the green and scalable nature of the method.[89–91]

As described in Fig. 6A, XRD patterns of the final material are dominated by the broad peaks typical of disordered carbon at 26° and 44°, indicative of graphitic (002) and (100) planes, respectively.[14] Minor crystalline phases are difficult to resolve by

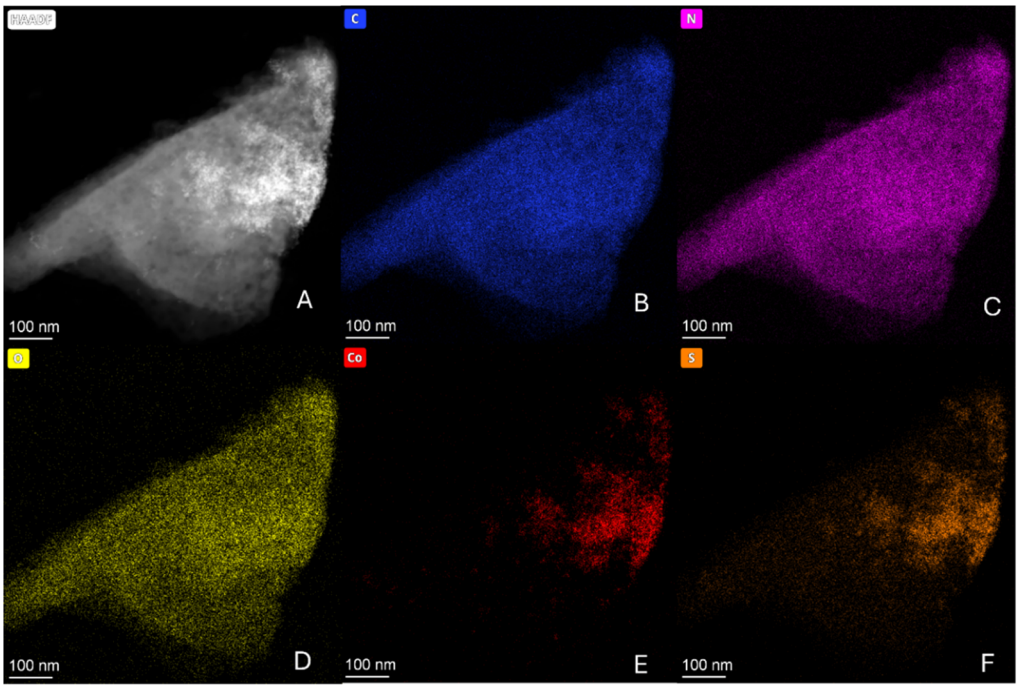

Fig. 5 STEM micrograph (A) and corresponding elemental mapping of (B) C, (C) N, (D) O, (E) Co, and (F) S of the catalyst.

XRD but are clearly identified through XPS (Fig. 6C–G). The C 1s spectrum evidences the coexistence of sp^2 carbon, oxygenated carbon species (C–O, C═O), and contributions from heteroatom doping. The N 1s region confirms the presence of pyridinic and graphitic nitrogen functionalities, which are known to influence catalytic behavior.[14,92,93] The O 1s signal indicates both lattice oxygen and oxygenated surface groups, while the S 2p spectrum confirms the retention of sulfur moieties within the material.[94] Finally, the Co 2p region shows characteristic Co signals of Co_3O_4 species anchored on the carbon surface.[95,96] Morphological characterization was further complemented by N_2 adsorption–desorption isotherms, which reveal a specific surface area of approximately 40 $m^2\ g^{-1}$. This value is particularly relevant given the absence of advanced morphological control strategies, porogenic agents, or solvent-based templating methods. The synthesis thus offers a robust, solvent-free, and waste-derived approach to catalyst design, scalable and environmentally benign, without generating secondary residues.

The catalytic upgrading of the non-condensable gases derived from pyrolysis over the catalyst resulted in clear modifications in gas composition (Fig. 6H). Relative to the direct pyrolysis gas, the catalytic stage led to a substantial enrichment in hydrogen and a strong depletion of condensable hydrocarbons, together with a redistribution of the carbon-containing species between CO_2 and CO. At 525 °C, the hydrogen fraction increased from 18 vol% in the raw pyrolysis gas to 32 vol% after catalytic treatment. At 650 °C, the gas composition reached 42.5% H_2, 18.7% CO_2, 20.0% CO, and 15.6% CH_4, with low levels of NH_3 and C_2–C_3 hydrocarbons. A further temperature increases to 750 °C produced a similar hydrogen fraction (43%), suggesting that the system approaches thermodynamic limits under the given feed composition. The marked enrichment in hydrogen is primarily attributed to cracking and dehydrogenation of CH_4 and C_2–C_3 hydrocarbons. The low concentrations of C_2 and C_3 at 650 °C indicate that these molecules are almost completely decomposed under catalytic conditions. In addition, ammonia decomposition contributes to hydrogen production, explaining the decrease in NH_3 at high temperatures. The parallel decrease of CO_2 and increase in CO can be partially ascribed the reverse water–gas shift (RWGS) reaction.[97] Although RWGS generates H_2O *in situ*, the concentration of steam is low, so steam reforming remains marginal under these conditions. The persistence of 15.6% CH_4 at 650 °C shows that methane decomposition is active but not complete,[98] and is counterbalanced by the dynamic equilibrium among RWGS and limited local methanation. The almost complete removal of C_2–C_3 confirms their susceptibility to scission, and the suppression of methanation at 650–750 °C prevents replenishment of CH_4 from $CO_x + H_2$. The structural and compositional features of the catalyst are key to enabling these transformations. Co-containing species dispersed at the carbon edges provide active sites for C–H and C–C bond activation, while the N- and O-doped carbon matrix enhances CO_2 adsorption and activation. The presence of residual sulfur functionalities can also modulate the electronic structure of the active sites, favoring coke tolerance when present at moderate levels. Despite its modest surface area (40 $m^2\ g^{-1}$), the catalyst offers sufficient dispersion of Co species and abundant defect sites to promote the reforming and cracking reactions. The resulting gas stream is competitive in terms of composition, resembling synthesis gas and offering strong potential for downstream valorization

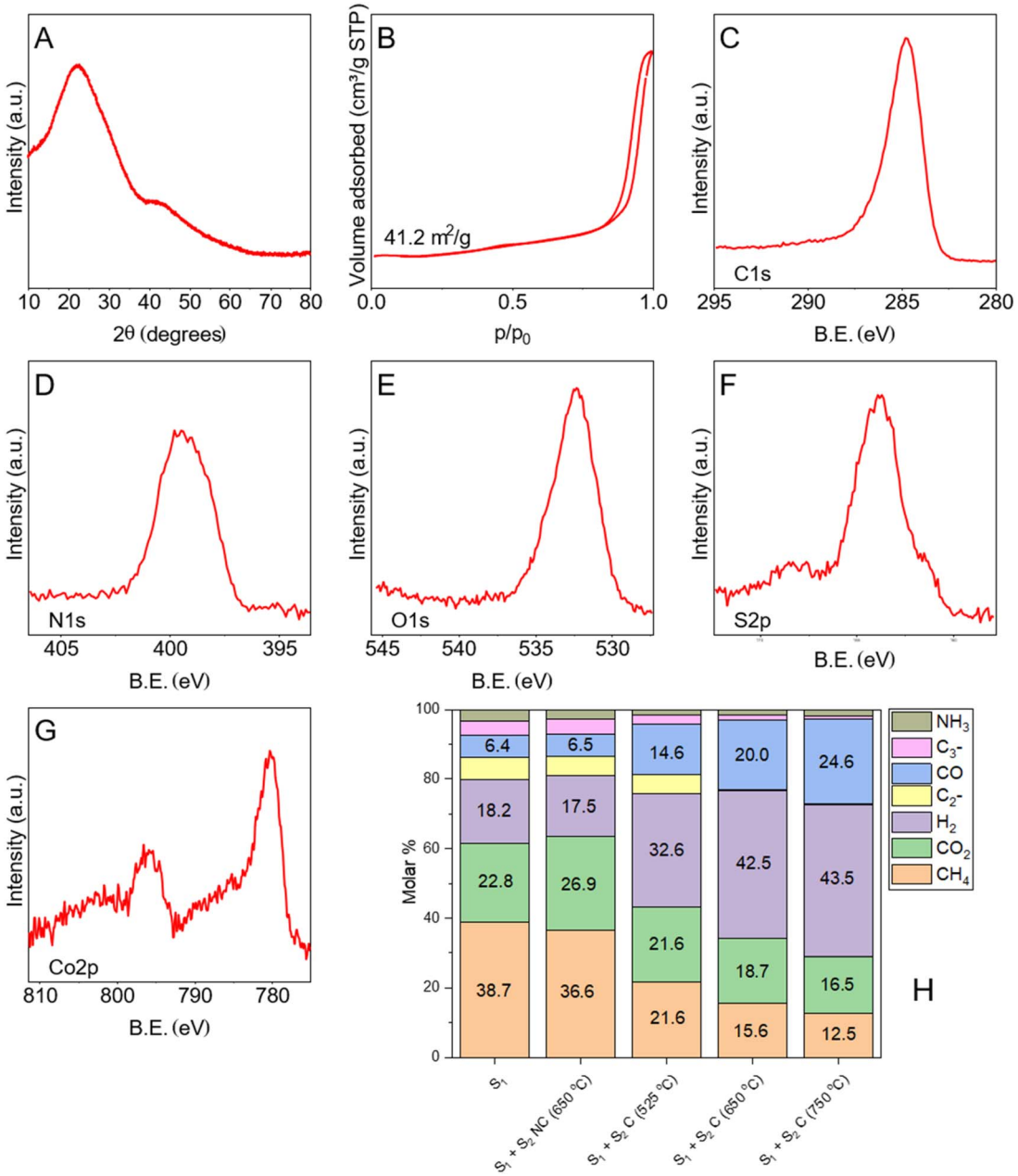

Fig. 6 Characterization data of the material synthesized from the char and liquid fractions. (A) X-ray diffraction patterns; (B) N_2 adsorption–desorption isotherms; (C–G) XPS spectra of the C 1s, N 1s, O 1s, S 2p, and Co 2p regions, respectively. (H) Catalytic performance results obtained in a two-step scheme (pyrolysis + catalytic transformation). S_1: step 1; S_2: step 2. NC refers to the reaction without catalyst (reference), whereas C corresponds to the reaction performed with the catalyst derived from residual fractions. The temperature values employed in step 2 are indicated, as well.

(42–43% H_2 with around 20% CO and more than 20% CO_2 at 650–750 °C). Additionally, two catalysts (Co/C and Pt/C) considered as relevant references were prepared and tested in this two-stage system. The gas composition results highlight the competitiveness of the catalyst obtained from the solid and liquid pyrolysis fractions (less valuable), as shown in Fig. S4. The material (C) derived from the pyrolysis fractions exhibited an H_2 concentration comparable to that obtained with the high-surface commercial carbon (Co/C). A decrease in hydrogen production was observed compared to the Pt/C sample. While such a reduction was anticipated due to the incorporation of a noble metal into the structure, it remained relatively modest, being limited to a factor of 1.3. In addition, the Co-based catalyst generated lower amounts of CO_2, representing a notable environmental advantage in terms of reduced greenhouse gas emissions.

From an economic perspective, the proposed valorization strategy, although developed at laboratory scale, is consistent with the current regulatory and market framework driving the transition toward circular economy models. In Spain, in line

with European regulations and the recommendations of most countries, Law 7/2022 together with Royal Decree 646/2020 on landfill disposal, establishes landfill as the least preferred option in the waste hierarchy and enforces progressive reduction targets for landfilling.[99,100] In addition, landfill taxation for bulky waste streams such as end-of-life mattresses is typically in the range of 40–100 € per tonne, which significantly increases the relative competitiveness of alternative treatment routes and strengthens the economic rationale for thermochemical valorization strategies. Within this context, chemical recycling technologies have been widely evaluated from a techno-economic perspective. According to recent comparative assessments, pyrolysis represents one of the most cost-competitive options, with estimated total costs (including CAPEX, OPEX, pre-treatment, and feedstock) of ~132 € per tonne, compared to higher values reported for gasification (~217 € per tonne), methanolysis (~292 € per tonne), glycolysis (~337 € per tonne), and depolymerisation (~350 € per tonne) under comparable system boundaries.[101] These differences are mainly attributed to the fact that pyrolysis and gasification are typically more capital expenditure (CAPEX)-driven, whereas glycolysis and depolymerisation are more operational expenditure (OPEX)-intensive due to reagent consumption, catalysts, and process complexity. However, despite its relative economic advantage, pyrolysis is still associated with relevant challenges, including significant energy demand, product upgrading requirements, and the need for efficient heat integration at scale. As highlighted in recent contributions, no single chemical recycling technology can be considered universally optimal, as each presents specific trade-offs in terms of cost, environmental impact, and product quality, requiring case-specific assessment depending on feedstock composition and desired outputs.[102–105] The integrated valorization of all pyrolysis-derived products should continue to be advanced, moving beyond single-stream exploitation toward full fraction utilization. In this context, the proposed materials synthesis scheme offers a viable outlet for the more challenging fractions, particularly the liquid and solid streams, which are typically associated with higher heteroatom content and lower direct market value.

The mechanochemical approach employed for catalyst preparation provides additional economic advantages, including solvent-free operation, reduced process complexity, and lower separation and purification requirements compared to conventional wet-chemistry routes.[106,107] Moreover, its reliance on mechanical energy input rather than extensive solvent use or multi-step processing can potentially translate into lower operational costs and improved scalability prospects. Therefore, this strategy not only enables the upgrading of low-value fractions into functional catalytic materials but also contributes to improving the overall economic feasibility of the proposed cascade valorization concept.

Despite the promising results obtained in this study, some limitations should be acknowledged. First, the pyrolysis experiments were performed at laboratory scale, and therefore the influence of heat and mass transfer constraints, as well as long-term operational stability, has not been fully addressed. The presence of nitrogen- and sulfur-containing compounds in both liquid and solid fractions also represent a limitation for direct downstream applications, particularly in refining contexts, and would require dedicated upgrading or removal strategies. For this reason, an alternative pathway toward the production of functional materials is proposed as a more suitable valorization route for these fractions. Furthermore, the catalytic performance, while competitive with a reference carbon-supported cobalt system, still shows a measurable gap compared to noble-metal-based catalysts, indicating room for further improvement in activity and selectivity. Besides, although the catalyst synthesis has been successfully demonstrated at laboratory scale, its scalability has not yet been experimentally validated beyond batch conditions. While the mechanochemical synthesis approach offers a promising route toward more scalable and solvent-free processing, further work is still required to assess its robustness under continuous or larger-scale operation and to confirm its reproducibility and process control under industrially relevant conditions. Overall, the study demonstrates an integrated and circular strategy for converting polyurethane-based waste mattresses into valuable gaseous products and catalytic materials, which, as evidenced in Table S1, has not been previously reported in the literature.

4. Conclusions

This work presents a two-step valorization strategy for waste mattresses, mainly composed of expanded polyurethane together with minor polymeric and textile fractions, integrating pyrolysis and catalytic upgrading of the resulting gas stream. Pyrolysis proved to be an effective route for the conversion of these complex residues, producing 12.6 wt% char, 55.1 wt% liquids, and 32.3 wt% gases at 525 °C. These results were obtained under the operating conditions that maximize the H_2 content in the gas fraction (525 °C, 13.1 °C min^{-1} and residence time of 60 min). The presence of PET and PP in mattress-cover mixtures increased char formation up to 23.5 wt% at the expense of liquid production, highlighting the strong influence of feedstock composition on product distribution.

The liquid fraction showed a complex and potentially valuable chemical composition. Elemental analysis indicated 56.1% C, 7.91% H, 4.67% N, and 0.01% S. Simulated distillation data revealed that 23.8% of the liquid corresponds to gasoline-range compounds, 27.4% to light cycle oil (LCO), and 48.8% to heavy cycle oil (HCO). A more detailed distribution showed the presence of light naphtha (5.2%), medium naphtha (2.6%), heavy naphtha (13.8%), kerosene (11.2%), distillate fuel oil (18.8%), light vacuum gas oil (33.5%), and heavy vacuum gas oil (14.9%). Although this broad hydrocarbon range highlights its potential as a refinery-compatible feedstock, the presence of heteroatoms limits its direct integration without further upgrading.

The solid fraction (char) exhibited a composition of 73.0% C, 3.3% H, 13.0% N, and 0.02% S, confirming its carbon-rich nature with significant nitrogen incorporation. Among all fractions, the gaseous product, mainly composed of CH_4, CO_2, H_2, and NH_3, showed the highest immediate potential for valorization. To further enhance the overall efficiency of the process, the solid and liquid fractions were successfully reused

as precursors for the preparation of a carbonaceous catalytic material doped with O and N and decorated with surface Co_3O_4 nanoparticles. The resulting catalyst exhibited a surface area of 40 m^2 g^{-1}, a noteworthy value considering that no porogenic agents, templating strategies, or solvent-based structuring methods were employed.

Catalytic upgrading of the pyrolysis gases significantly improved gas quality, increasing the H_2 concentration from 18 vol% to 42.5 vol% at 650 °C while simultaneously reducing CO_2, NH_3, and light hydrocarbons, thus shifting the composition towards a more syngas-like mixture. Importantly, the catalyst derived from pyrolysis fractions exhibited catalytic performance comparable to reference Co/C catalyst prepared using commercial carbon supports, and only slightly lower than that of Pt/C, while generating lower CO_2 emissions.

Author contributions

M. C.: conceptualization, investigation, methodology, formal analysis, supervision, writing – review and editing, funding acquisition. A. P.-M.: investigation, formal analysis, writing – original draft. R. R. S.: investigation, writing – review and editing, validation. G. B.: methodology, investigation, methodology, formal analysis, conceptualization, supervision. M. J. M.-B.: conceptualization, investigation, methodology, formal analysis, supervision, writing – original draft, writing – review and editing, funding acquisition.

Conflicts of interest

The authors declare that they have no known competing financial interests or personal relationships that could have appeared to influence the work reported in this paper.

Abbreviations

ASTM	American Society for Testing and Materials
C	Waste derived catalyst (N,O, S-Co_3O_4/C)
C_A and C_B	Coating samples
CASE	Coatings, adhesives, sealants, and elastomers
Co/C	Co_3O_4/commercial carbon catalyst (reference)
DOE	Design of experiments
DTG	Derivative thermogravimetric
EDX	Energy-dispersive X-ray
FID	Flame ionization detector
FTIR	Fourier-transform infrared spectroscopy
GC	Gas chromatography
GC-MS	Gas chromatography coupled to mass spectrometry
HAADF	High-angle annular dark field
HCO	Heavy cycle oil
IC	Ion current
LCO	Light cycle oil
MS	Mass spectrometry
NIST	National Institute of Standards and Technology
PE	Polyethylene
PET	Polyethylene terephthalate
PP	Polypropylene
PU	Polyurethane
PU_A	Monolayer polyurethane samples
PU_{B1}–PU_{B3}	Multilayer polyurethane mattresses samples
Pt/C	Pt/commercial carbon catalyst (reference)
RWGS	Reverse water–gas shift
S_{BET}	Specific surface area (Brunauer–Emmett–Teller method)
SD	Standard deviation
STEM	Scanning transmission electron microscopy
TGA	Thermogravimetric analysis
V_T	Total pore volume
XPS	X-ray photoelectron spectroscopy
XRD	X-ray diffraction

Data availability

The data supporting this article have been included in the main document or as part of the supplementary information (SI). Supplementary information: additional characterization data for the waste mattress and pyrolysis-derived liquids, catalytic performance benchmark data, and a literature overview of polyurethane and waste mattress pyrolysis. See DOI: https://doi.org/10.1039/d6su00099a.

Acknowledgements

This work has received funds from the project PID2022-139014OB-I00/SRA (State Research Agency)/10.13039/501100011033. Authors thank the Delegation of Water, Agrarian Promotion and Environment of the Provincial Council of Granada, and the Planning Section, for the implementation of actions aimed at improving the circular economy in the Province of Granada. The authors also acknowledge Ecocentral Granada, owned by the Provincial Council of Granada, and FCC (Fomento de Construcciones y Contratas, S.A., Spain) for their collaboration in providing the waste samples used in this work. The authors also thank the CIC (Centro de Instrumentación Científica) of the University of Granada and STI (Servicios Técnicos de Investigación) of the University of Alicante, where part of the characterization experiments was carried out. Funding for open access charge: Universidad de Granada/CBUA.

References

1 P. G. C. Nayanathara Thathsarani Pilapitiya and A. S. Ratnayake, *Cleaner Mater.*, 2024, **11**, 100220.
2 A. Kemona and M. Piotrowska, *Polymers*, 2020, **12**, 1752.
3 A. Das and P. Mahanwar, *Adv. Ind. Eng. Polym. Res.*, 2020, **3**, 93–101.
4 A. Magnin, E. Pollet, V. Phalip and L. Avérous, *Biotechnol. Adv.*, 2020, **39**, 107457.
5 E. Pęczek, R. Pamuła and A. Białowiec, *Materials*, 2024, **17**, 1013.

6 W. Wang and C. Wang, in *The Design and Manufacture of Medical Devices*, Elsevier, 2012, pp. 115–151.
7 A. Rafiee, K. Rajab Khalilpour, D. Milani and M. Panahi, *J. Environ. Chem. Eng.*, 2018, **6**, 5771–5794.
8 C. Gamerith, E. Herrero Acero, A. Pellis, A. Ortner, R. Vielnascher, D. Luschnig, B. Zartl, K. Haernvall, S. Zitzenbacher, G. Strohmeier, O. Hoff, G. Steinkellner, K. Gruber, D. Ribitsch and G. M. Guebitz, *Polym. Degrad. Stab.*, 2016, **132**, 69–77.
9 M. Tessman, B. Kuntasal and M. Modi, in *Rethinking Polyester Polyurethanes*, Elsevier, 2023, pp. 127–151.
10 Europur, *The End-of-Life of Flexible Polyurethane Foam from Mattresses and Furniture*, 2021.
11 *Enabling the Recycling of Foam Mattresses – cefic.org*, https://cefic.org/a-solution-provider-for-sustainability/chemical-recycling-making-plastics-circular/chemical-recycling-via-depolymerisation-to-monomer/enabling-the-recycling-of-foam-mattresses, accessed 25 April 2025.
12 Evonik, *Evonik partners with the Vita Group for Pioneering Efficient Polyurethane Mattress Recycling Process – Evonik Industries*, https://www.pu-additives.com/en/evonik-partners-with-the-vita-group-for-pioneering-efficient-polyurethane-mattress-recycling-process-165382.html, accessed 25 April 2025.
13 J. Fathi, M. Hlína, T. Mates, M. Buryi, V. S. Sikarwar, R. Mušálek, S. Sharma, M. Lojka, A. Jiříčková, O. Jankovský, J. Riedl, M. Karlík, P. Kratochvíl, H. Thürlová, F. Růzička, F. Průša, M. Jeremiáš and A. Mašláni, *Chem. Eng. J.*, 2025, **511**, 161910.
14 M. Calero, G. Blázquez, R. R. Solís, M. Á. Martín-Lara and M. J. Muñoz-Batista, *Chem. Eng. J.*, 2025, **503**, 158244.
15 G. Botla, P. Barmavatu, M. Pohorely, M. Jeremias and V. S. Sikarwar, *Therm. Sci. Eng. Prog.*, 2024, **50**, 102514.
16 K. M. Zia, H. N. Bhatti and I. Ahmad Bhatti, *React. Funct. Polym.*, 2007, **67**, 675–692.
17 G. Rossignolo, G. Malucelli and A. Lorenzetti, *Green Chem.*, 2024, **26**, 1132–1152.
18 T. Lee, D. Kwon, S. Lee, Y. Kim, J. Y. Kim, H. Song, S. Jung, J. Lee, Y. F. Tsang, K.-H. Kim and E. E. Kwon, *Prog. Energy Combust. Sci.*, 2025, **108**, 101219.
19 M. A. Quintana, G. Garcia-Garcia, G. Blazquez, M. A. Martín-Lara, M. Calero and M. J. Muñoz-Batista, *J. Anal. Appl. Pyrolysis*, 2026, **193**, 107480.
20 U. S. Behera, S. Poddar and H.-S. Byun, *Sustainable Energy Fuels*, 2025, **9**, 4103–4124.
21 M. M. Hasan, R. Haque, M. I. Jahirul and M. G. Rasul, *Energy Convers. Manage.*, 2025, **326**, 119511.
22 W.-H. Chen, P. Pratim Biswas, E. E. Kwon, Y.-K. Park, S. Rajendran, L. Gnanasekaran and J.-S. Chang, *Chem. Eng. J.*, 2023, **471**, 144695.
23 T. Lee, S. Jung, S. Lee, Y. F. Tsang, K. H. Lee and E. E. Kwon, *Energy Convers. Manage.*, 2024, **315**, 118827.
24 M. J. Muñoz-Batista, G. Blázquez, R. R. Solís, A. Pérez, M. Á. Martín-Lara and M. Calero, *ACS ES&T Eng.*, 2025, **5**, 22–35.
25 M. Calero, R. R. Solís, M. J. Muñoz-Batista, A. Pérez, G. Blázquez and M. Ángeles Martín-Lara, *Chem. Eng. Sci.*, 2023, **271**, 118569.
26 Y. Misra, D. J. Prasanna Kumar, R. K. Mishra, V. Kumar and N. Dwivedi, *Water-Energy Nexus*, 2025, **8**, 55–72.
27 M. Hashemi, K. T. Q. Nguyen, D. J. Robert, G. K. Zhang, T. Hosseinnejad and D. Marney, *J. Anal. Appl. Pyrolysis*, 2026, **193**, 107360.
28 Y. Zhang, C. Liu, G. Ji, Z. Ma, A. Li and H. Zhang, *Fuel*, 2026, **404**, 136235.
29 S. van Wyk, C. F. Mourao Vilela and B. J. Vreugdenhil, *Fuel*, 2026, **407**, 137564.
30 T. Lee, H. Cha, S. Lee, J. Lee and E. E. Kwon, *Energy*, 2025, **319**, 135053.
31 S. H. Cho, J. Park, S. Jung, D. Lee and E. E. Kwon, *J. Anal. Appl. Pyrolysis*, 2024, **181**, 106638.
32 P. Moonsin, W. Roschat, S. Phewphong, S. Watthanalao, P. Chaona, B. Maneerat, S. Arthan, A. Thammayod, T. Leelatam, K. Duanguppama, B. Yoosuk, P. Janetaisong and V. Promarak, *J. Taiwan Inst. Chem. Eng.*, 2025, **171**, 106040.
33 Y. Hu, J. Zhou, Q. Qian and J. Ren, *Energy*, 2025, **323**, 135812.
34 J. A. Conesa and E. Tomás, *Sci*, 2022, **4**, 48.
35 R. Gómez-Rojo, L. Alameda, Á. Rodríguez, V. Calderón and S. Gutiérrez-González, *Polymers*, 2019, **11**, 359.
36 M. Modesti, F. Simioni, R. Munari and N. Baldoin, *React. Funct. Polym.*, 1995, **26**, 157–165.
37 D. Simón, A. M. Borreguero, A. de Lucas and J. F. Rodríguez, *Waste Manage.*, 2018, **76**, 147–171.
38 D. Simón, A. M. Borreguero, A. de Lucas, C. Gutiérrez and J. F. Rodríguez, in *Handbook of Environmental Chemistry*, Springer Verlag, 2014, vol. 32, pp. 229–260.
39 J. M. Orts, E. Naranjo, S. Pina, A. Orts, M. Muñoz-Martí, M. Tejada and J. Parrado, *Bioresour. Technol.*, 2025, **416**, 131814.
40 J. Oenema, H. Liu, N. De Coensel, A. Eschenbacher, R. Van de Vijver, J. Weng, L. Li, C. Wang and K. M. Van Geem, *J. Anal. Appl. Pyrolysis*, 2022, **168**, 105723.
41 R. Hasanzadeh, P. Mojaver, S. Khalilarya, T. Azdast, A. Chitsaz and M. Mojaver, *Polymers*, 2022, **14**, 4938.
42 R. Font, A. Fullana, J. A. Caballero, J. Candela and A. García, *J. Anal. Appl. Pyrolysis*, 2001, **58–59**, 63–77.
43 A. Veses, O. Sanahuja-Parejo, I. Martínez, M. S. Callén, J. M. López, T. García and R. Murillo, *Waste Manage.*, 2021, **120**, 415–423.
44 D. Serrano, A. Horvat, R. M. Mata, P. Costa and F. Paraleda, *Waste Manage.*, 2024, **181**, 11–19.
45 M. A. Garrido, R. Font and J. A. Conesa, *Waste Manage.*, 2016, **52**, 138–146.
46 M. A. Garrido and R. Font, *J. Anal. Appl. Pyrolysis*, 2015, **113**, 202–215.
47 H. A. Sani, M. Muhammad, A. Muhammad and T. A. Saleh, *Next Sustainability*, 2024, **3**, 100024.
48 M. Zeller, D. Merz, L. Weigel, S. Tavakkol and D. Stapf, *J. Anal. Appl. Pyrolysis*, 2025, **188**, 107048.

49 Y. Nishiyama, S. Kumagai, S. Motokucho, T. Kameda, Y. Saito, A. Watanabe, H. Nakatani and T. Yoshioka, *J. Anal. Appl. Pyrolysis*, 2020, **145**, 104754.
50 Q. Chen, T. B. Y. Chen, W. J. Yang, I. M. De Cachinho Cordeiro and R. K. K. Yuen, *Composites, Part A*, 2026, **207**, 109854.
51 U. Caudillo-Flores, M. J. Muñoz-Batista, A. Kubacka and M. Fernández-García, *Mol. Catal.*, 2020, **481**, 110240.
52 U. Caudillo-Flores, I. Barba-Nieto, M. J. Muñoz-Batista, D. Motta Meira, M. Fernández-García and A. Kubacka, *Chem. Eng. J.*, 2021, **425**, 130641.
53 J. P. Lewicki, K. Pielichowski, P. T. De La Croix, B. Janowski, D. Todd and J. J. Liggat, *Polym. Degrad. Stab.*, 2010, **95**, 1099–1105.
54 J. Pagacz, E. Hebda, B. Janowski, D. Sternik, M. Jancia and K. Pielichowski, *Polym. Degrad. Stab.*, 2018, **149**, 129–142.
55 D. K. Chattopadhyay and D. C. Webster, *Prog. Polym. Sci.*, 2009, **34**, 1068–1133.
56 D. Włodarczak, *J. Appl. Polym. Sci.*, 1988, **36**, 377–386.
57 M. Herrera, G. Matuschek and A. Kettrup, *Polym. Degrad. Stab.*, 2002, **78**, 323–331.
58 R. Alshareef, M. A. Nahil and P. T. Williams, *Energy Fuels*, 2023, **37**, 3894–3907.
59 K. Krempl, D. Hochfilzer, F. Cavalca, M. Saccoccio, J. Kibsgaard, P. C. K. Vesborg and I. Chorkendorff, *ChemElectroChem*, 2022, **9**, e202101713.
60 B. Zheng, Y. Li, H. Ma, G. Chen, Y. Gu and C. Wang, *J. Anal. Appl. Pyrolysis*, 2024, **179**, 106497.
61 X. Gu, X. Ma, L. Li, C. Liu, K. Cheng and Z. Li, *J. Anal. Appl. Pyrolysis*, 2013, **102**, 16–23.
62 E. G. Krukowski, A. Goodman, G. Rother, E. S. Ilton, G. Guthrie and R. J. Bodnar, *Appl. Clay Sci.*, 2015, **114**, 61–68.
63 D. K. Schneiderman, M. E. Vanderlaan, A. M. Mannion, T. R. Panthani, D. C. Batiste, J. Z. Wang, F. S. Bates, C. W. Macosko and M. A. Hillmyer, *ACS Macro Lett.*, 2016, **5**, 515–518.
64 L. Jiao, H. Xiao, Q. Wang and J. Sun, *Polym. Degrad. Stab.*, 2013, **98**, 2687–2696.
65 X. Zhao, J. Wang, J. Li and Q. Yu, *J. Anal. Appl. Pyrolysis*, 2024, **177**, 106279.
66 Z. Shah, M. Gulzar, F. Hasan and A. A. Shah, *Polym. Degrad. Stab.*, 2016, **134**, 349–356.
67 L. Tao, G.-B. Zhao, J. Qian and Y. Qin, *J. Hazard. Mater.*, 2010, **175**, 754–761.
68 S. Pasieczna-Patkowska, M. Cichy and J. Flieger, *Molecules*, 2025, **30**, 684.
69 J. Datta, P. Kosiorek and M. Włoch, *J. Therm. Anal. Calorim.*, 2017, **128**, 155–167.
70 M. Snels, A. Beil, H. Hollenstein and M. Quack, *Chem. Phys.*, 1997, **225**, 107–130.
71 M. F. Paucar-Sánchez, M. A. Martín-Lara, M. Calero, G. Blázquez, R. R. Solís and M. J. Muñoz-Batista, *Fuel*, 2023, **352**, 129145.
72 S. Sá e Sant'Anna, D. A. de Souza, D. M. de Araujo, C. de Freitas Carvalho and M. I. Yoshida, *Mater. Res.*, 2008, **11**, 433–438.
73 M. Ates, S. Karadag, A. A. Eker and B. Eker, *Polym. Int.*, 2022, **71**, 1157–1163.
74 V. Singh, M. N. Gopalasamudram and J. Maitra, *Polym. Adv. Technol.*, 2024, **35**, e6313.
75 M. Smith, L. Scudiero, J. Espinal, J. S. McEwen and M. Garcia-Perez, *Carbon*, 2016, **110**, 155–171.
76 A. P. Dementjev, A. de Graaf, M. C. M. van de Sanden, K. I. Maslakov, A. V. Naumkin and A. A. Serov, *Diamond Relat. Mater.*, 2000, **9**, 1904–1907.
77 R. Pietrzak, *Fuel*, 2009, **88**, 1871–1877.
78 T. H. Qin, G. Ji, B. Qu, A. J. McCue, S. Guan, J. Derksen and Y. S. Zhang, *Carbon Capture Sci. Technol.*, 2025, **14**, 100382.
79 J. Wu, X. He, L. Xu, Q. Song, Z. Tian, C. Wang, M. Zhao, G. Zhou and Y. Gao, *Int. J. Hydrogen Energy*, 2025, **142**, 1102–1112.
80 Y. Li, M. A. Nahil and P. T. Williams, *Chem. Eng. J.*, 2023, **467**, 143427.
81 J. Alvarez, S. Kumagai, C. Wu, T. Yoshioka, J. Bilbao, M. Olazar and P. T. Williams, *Int. J. Hydrogen Energy*, 2014, **39**, 10883–10891.
82 M. Lahafdoozian, H. Khoshkroudmansouri, S. H. Zein and A. A. Jalil, *Int. J. Hydrogen Energy*, 2024, **59**, 465–479.
83 L. F. Liotta, H. Wu, G. Pantaleo and A. M. Venezia, *Catal. Sci. Technol.*, 2013, **3**, 3085.
84 M. Khasu, T. Nyathi, D. J. Morgan, G. J. Hutchings, M. Claeys and N. Fischer, *Catal. Sci. Technol.*, 2017, **7**, 4806–4817.
85 F. Ortega, L. Jiménez-Rodríguez, G. Blázquez, M. Calero and M. J. Muñoz-Batista, *J. Environ. Chem. Eng.*, 2026, **14**, 121775.
86 D. Yuan, Y. Dou, C. T. He, L. Yu, L. Xu, D. Adekoya, Q. Xia, J. Ma, S. X. Dou and S. Zhang, *Cell Rep. Phys. Sci.*, 2021, **2**, 100331.
87 C. Maouche, J. Yang, S. H. Al-Hilfi, X. Tao and Y. Zhou, *ACS Appl. Nano Mater.*, 2022, **5**, 4397–4405.
88 W. Wang, H. Zhao, X. Zhao, J. Rong, N. Liu, P. Yu, J. Xie, G. Wu, H. Li, M. Xin and M. Zong, *Catal. Today*, 2024, **433**, 114691.
89 O. Trentin, M. J. Muñoz-Batista, A. Perosa, M. Selva and D. Rodriguez-Padron, *Adv. Funct. Mater.*, 2025, e06860.
90 X. Liu, Y. Li, L. Zeng, X. Li, N. Chen, S. Bai, H. He, Q. Wang and C. Zhang, *Adv. Mater.*, 2022, **34**, 2108327.
91 M. J. Muñoz-Batista, D. Rodríguez-Padrón, A. R. Puente-Santiago and R. Luque, *ACS Sustain. Chem. Eng.*, 2018, **6**, 9530–9544.
92 W. H. Lee, J. Y. Kim, Y. K. Ko, P. J. Reucroft and J. W. Zondlo, *Appl. Surf. Sci.*, 1999, **141**, 107–113.
93 A. Ligero, R. R. Solís, G. Blázquez, M. J. Muñoz-Batista, A. Pérez and M. Calero, *J. Environ. Chem. Eng.*, 2024, **12**, 112265.
94 J. C. Ruiz-Cornejo, D. Sebastián, J. I. Pardo, M. V. Martínez-Huerta and M. J. Lázaro, *J. Power Sources*, 2022, **546**, 231988.
95 J. Huang, W. Qian, H. Ma, H. Zhang and W. Ying, *RSC Adv.*, 2017, **7**, 33441–33449.
96 S. N. F. Moridon, M. I. Salehmin, M. A. Mohamed, K. Arifin, L. J. Minggu and M. B. Kassim, *Int. J. Hydrogen Energy*, 2019, **44**, 25495–25504.

97 R. Alshareef, M. A. Nahil and P. T. Williams, *Energy Fuels*, 2023, **37**, 3894–3907.
98 L. Alves, V. Pereira, T. Lagarteira and A. Mendes, *Renewable Sustainable Energy Rev.*, 2021, **137**, 110465.
99 *BOE-A-2022-5809 Ley 7/2022, de 8 de abril, de residuos y suelos contaminados para una economía circular*, https://www.boe.es/buscar/act.php?id=BOE-A-2022-5809, accessed 20 May 2026.
100 *BOE-A-2020-7438 Real Decreto 646/2020, de 7 de julio, por el que se regula la eliminación de residuos mediante depósito en vertedero*, https://www.boe.es/buscar/doc.php?id=BOE-A-2020-7438, accessed 20 May 2026.
101 D. Caro, P. F. Albizzati, J. Cristobal Garcia, I. Saputra Lase, P. Garcia-Gutierrez, R. Juchtmans, E. Garbarino, G. Blengini, S. Manfredi, S. De Meester, and D. Tonini, *Towards a Better Definition and Calculation of Recycling – Proposals for Calculating Recycling Yields in Multi-Output Processes and Recycling of Biodegradable Waste, and a QualityFramework for Recycling*, Publications Office of the European Union, 2023, https://data.europa.eu/doi/10.2760/636900.
102 K. Wieczorek, P. Bukowski, K. Stawiński and I. Ryłko, *Materials*, 2024, **17**, 4617.
103 A. N. Srivastava, V. S. Sikarwar, D. Bisen, J. Fathi, A. Maslani, B. N. Lopez Nino, P. Barmavatu, A. K. Kaviti, M. Pohořelý and M. Buryi, *Processes*, 2025, **13**, 2014.
104 I. Harasymchuk, V. Kočí and M. Vitvarová, *Int. J. Sustain. Eng.*, 2024, **17**, 124–148.
105 S. Swami, S. Suthar, R. Singh, A. K. Thakur, L. R. Gupta and V. S. Sikarwar, *Environ. Dev. Sustain.*, 2023, **27**(5), 9773–9803.
106 S. R. Wenger, E. R. Kearns, K. L. Miller and D. M. D'Alessandro, *ACS Appl. Energy Mater.*, 2023, **6**, 9074–9083.
107 J. F. Reynes, V. Isoni and F. García, *Angew. Chem., Int. Ed.*, 2023, **62**, e202300819.